Groundwater

Continental Scale Hydrostratigraphy: Basin-Scale Testing of Alternative Data-Driven Approaches

by Danielle Tijerina-Kreuzer^{1,2}, Jackson S. Swilley^{1,3}, Hoang V. Tran⁴, Jun Zhang^{5,6}, Benjamin West⁵, Chen Yang^{1,3}, Laura E. Condon⁵, and Reed M. Maxwell^{1,3,7}

Abstract

Integrated hydrological modeling is an effective method for understanding interactions between parts of the hydrologic cycle, quantifying water resources, and furthering knowledge of hydrologic processes. However, these models are dependent on robust and accurate datasets that physically represent spatial characteristics as model inputs. This study evaluates multiple data-driven approaches for estimating hydraulic conductivity and subsurface properties at the continental-scale, constructed from existing subsurface dataset components. Each subsurface configuration represents upper (unconfined) hydrogeology, lower (confined) hydrogeology, and the presence of a vertical flow barrier. Configurations are tested in two large-scale U.S. watersheds using an integrated model. Model results are compared to observed streamflow and steady state water table depth (WTD). We provide model results for a range of configurations and show that both WTD and surface water partitioning are important indicators of performance. We also show that geology data source, total subsurface depth, anisotropy, and inclusion of a vertical flow barrier are the most important considerations for subsurface configurations. While a range of configurations proved viable, we provide a recommended Selected National Configuration 1 km resolution subsurface dataset for use in distributed large-and continental-scale hydrologic modeling.

Introduction

Hydrological modeling is commonly used to better understand the distribution of water resources on the

¹Integrated GroundWater Modeling Center, Princeton University, Princeton, NJ

Received January 2023, accepted September 2023.

© 2023 The Authors. *Groundwater* published by Wiley Periodicals LLC on behalf of National Ground Water Association.

This is an open access article under the terms of the Creative Commons Attribution-NonCommercial License, which permits use, distribution and reproduction in any medium, provided the original work is properly cited and is not used for commercial purposes.

doi: 10.1111/gwat.13357

Earth. These models can help to represent hydrogeologic processes and quantify groundwater, which is essential for a thorough knowledge of the hydrologic system. The quality of groundwater simulation within models is highly dependent on having the accuracy of the subsurface datasets. This is particularly challenging when modeling water resources across at continental scales because of the of lack large-scale, seamless subsurface datasets (Gleeson et al. 2014, 2021; Maxwell et al. 2015; Condon et al. 2021).

While many studies have tested sensitivity to hydraulic conductivity generally (e.g., Araya and Ghezzehei 2019; de Pue et al. 2019; Foster and Maxwell 2019), sensitivity to parameters is tested within a single assumed geologic structure and it is less common to explore larger uncertainty in the geologic framework itself. This is a type of model uncertainty that is rarely tested yet may play an important role in model performance (Enemark et al. 2019). Given the importance of hydraulic conductivity on not only groundwater flow but also streamflow (e.g., Srivastava et al. 2014; Foster and Maxwell 2019; Abimbola et al. 2020) and the challenges large-scale models face in reproducing water table depth observations (e.g., Reinecke et al. 2020), the development and evaluation of large-scale hydrostratographic datasets

NGWA.org Groundwater

²Corresponding author: Department of Civil and Environmental Engineering, Princeton University, Princeton, NJ; dtijerina@princeton.edu

³Department of Civil and Environmental Engineering, Princeton University, Princeton, NJ

⁴Atmospheric Science and Global Change Division, Pacific Northwest National Laboratory, Richland, WA

⁵Department of Hydrology and Atmospheric Sciences, University of Arizona, Tucson, AZ

⁶Key Laboratory of VGE of Ministry of Education, Nanjing Normal University, Nanjing, China

⁷High Meadows Environmental Institute, Princeton University, Princeton, N.I.

Article impact statement: The development and evaluation of several data-driven subsurface products in two test domains inform a national configuration for hydrostratigraphy.

is an ongoing community effort (e.g., Condon et al. 2021; Gleeson et al. 2021).

The purpose of this study is to compile a nationally consistent hydrostratigraphy dataset (i.e., the geologic properties below the soil) from existing subsurface datasets for use in continental-scale hydrological modeling applications. To accomplish this, we generate various subsurface configurations constructed from published subsurface datasets and evaluate the performance of these configurations using an integrated, hydrologic model in two regional test subdomains. We provide an open source and validated subsurface dataset for the continental United States based on a data-driven approach with the most current available data (Condon et al. 2020, 2021; Zell and Sanford 2020; Gleeson et al. 2021). We present a Selected National Configuration that we find is an optimal and seamless subsurface conceptual model for the continental United States (U.S.) and that will undergo additional testing in a high-resolution, integrated hydrological model over the contiguous United States.

Background

The primary goal of this study is to further understanding of the way that subsurface permeability is characterized in large-scale hydrological models. Immense amounts of observational data are needed to accurately represent these different components of the subsurface across continental scales. Unfortunately, subsurface data in the United States often collected and made available at the discretion of local or state entities (Maxwell et al. 2015). Therefore, there are few continuous and seamless subsurface datasets available for the entire United States (Condon et al. 2021).

A growing number of datasets do exist at the global and continental scale that characterize subsurface properties and that are relevant to this study. Gleeson et al. (2014) and Huscroft et al. (2018) have developed spatially distributed global permeability maps with the Global Hydrogeology MaPS 1.0 and 2.0 (henceforth referred to as *GLHYMPS 1.0* and *GLHYMPS 2.0*). The U.S. Geological Survey (USGS) has extensively mapped primary aquifer systems over the North American continent (Back et al. 1988; USGS 2003) and has more recently expanded these maps to include Secondary Hydrogeologic Regions (Belitz et al. 2019), which characterizes the hydrogeologic regions outside of the Primary Aquifers by lithology and geologic age.

Beyond classification of geologic types, work has been completed to characterize depth to bedrock. Shangguan et al. (2017) provided a global estimate of unconsolidated material depth at a spatial resolution of 250 m and an absolute depth to bedrock up to 540 m. Pelletier et al. (2016) quantified spatial variations in unweathered bedrock up to 50 m in depth.

Finally, soil is an integral component of the subsurface system. While there are various soil products available for the CONUS, the main United States soil surveys are STATSGO and SSURGO (Soil Survey Staff,

NRCS), the latter being the highest detail soil survey in the United States (Chaney et al. 2019). Outside of the United States, the gridded Global Soil Dataset for use in Earth System Models (GSDE) (Shangguan et al. 2014; Dai et al. 2019b, 2019c) uses various regional soil data to compile a global soils dataset. Soil is a well-documented component of the subsurface with many of the previously mentioned datasets having undergone evaluation and comparison (Wang and Melesse 2006; Mednick et al. 2008; Williamson et al. 2013; Dai et al. 2019a).

It is worth an additional mention that there are analytical approaches to estimate subsurface properties that we do not focus on in this study. For example, de Graaf et al. developed continental aquifer parameterizations based on local hydrogeological data (de Graaf et al. 2020), Gupta et al., Montzka et al., and Jarvis et al., estimate hydraulic properties from soil using pedotransfer functions (Jarvis et al. 2013; Montzka et al. 2017; Gupta et al. 2021), and Luo et al. and Tashie et al. estimate hydraulic conductivity with analytical approaches (Luo et al. 2010; Tashie et al. 2021). While these methodologies are valuable, we focus on data-driven approaches in this study; a companion article evaluates analytical approaches such as the Luo et al-type compared to data-driven approaches (Swilley et al. this issue).

Methods

When considering how to physically represent the subsurface, there is a range of complexity to consider. Figure 1 depicts important components of the hydrogeologic structure in a conceptual model that was used to organize the different test cases considered in this study. While this figure simplifies properties of the subsurface for the purpose of large-scale modeling, the following section describes the conceptual model and the important hydrostratigraphic components relevant at continental-scales.

The soil column comprises the uppermost layer, usually representing the top one to two meters of the

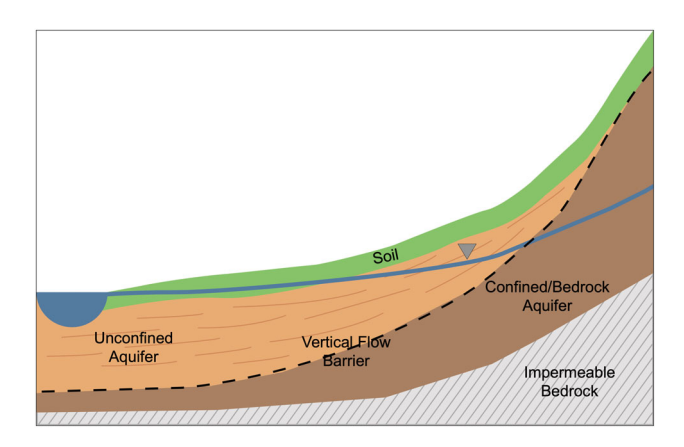


Figure 1. Conceptual model of the most pertinent subsurface properties addressed in this paper. Because this is a conceptual diagram, impacts to water table behavior may not be explicitly represented.

subsurface. At the bottom of the subsurface is impermeable bedrock, typically used as a no-flow boundary in hydrologic models and acts as a true no-flow layer. Between the soil and bedrock are heterogeneous geologic materials, represented as upper and lower geologies of unconfined and confined aquifer systems, respectively. While these geologies are mapped as specific types, the boundary between unconfined and confined aquifer systems is further delineated with a confining layer (referred to in this study as a vertical flow barrier).

There are additional considerations needed to depict a more realistic hydrostratigraphy, for example, within these geologic materials, anisotropy may be considered to better represent preferential flow as a result of stratification. Additionally, because hydrologic conductivity varies depending on slope, another component to consider is the e-folding relationship between terrain slope and hydrologic conductivity decay with subsurface depth (Fan et al. 2007).

We acknowledge that this conceptual model is a simplification of the underlying geology across the United States. It best represents regions where confined aquifers are bedrock aquifers, such as the intermountain west; or areas where a distinct confining layer exists, such as over the north-central United States. Other regions may be poorly represented by this conceptual model. Examples include previously glaciated areas or regions with extensive fine-grain, alluvial deposits, such as the Mississippi Alluvial Plain (Gratzer et al. 2020). We use this model to describe the tests conducted in this study and conceptualize how the subsurface might be configured within a continental-scale hydrology simulation.

Datasets

Using a selection of previously published hydrogeological data in conjunction with our conceptual subsurface model, we create combinations of the different subsurface datasets to test the viability of several configurations. In this study, the test datasets consist of GLHYMPS 1.0, GLHYMPS 2.0, and USGS (a combination of the Primary Aquifers map and the Secondary Hydrogeologic Regions map) for the upper and lower geology mapping, as well as the Shangguan depth to bedrock dataset. Our approach combines, reprojects, and resamples these different gridded datasets to the simulation grid to test different inputs of our conceptual model by comparing simulation results from two real world domains. It should be noted that while many of these datasets have been used extensively for a range of applications (e.g., Sutanudjaja et al. 2014; de Graaf et al. 2015; Maxwell and Condon 2016; Hellwig et al. 2020; Coon and Shuai 2022), to our knowledge, no comprehensive evaluation to hydrologic observations has been completed.

For the lower geology below the soil, three datasets are tested. First, *GLHYMPS 1.0* globally maps permeability and porosity at high resolutions with an average polygon size of about 100 km² (Gleeson et al. 2014).

This dataset is a synthesis of global permeability and lithology maps. GLHYMPS 2.0 is an improved permeability mapping of the initial GLHYMPS 1.0 dataset, resulting in a two-layer permeability maps of global unconsolidated sediments (Huscroft et al. 2018). The third dataset is a combination of the USGS Primary Aquifer system and the Secondary Hydrogeologic Regions. The Primary Aguifer system maps the most productive aguifers in the United States, but only account for about 60% of the conterminous United States. The Secondary Hydrogeologic Regions is a complementary dataset that characterizes the other 40% of the Primary Aquifer system map. The average polygon size for the Secondary Hydrogeologic Regions is 46,000 km² (Belitz et al. 2019). For this study, these datasets are combined to describe continental hydrostratigraphy and are henceforth referred to as USGS.

An important attribute we test in this study is the presence of a vertical flow barrier, which emulates a physical delineation and vertical flow reduction between unconfined and confined aquifers. Depth to bedrock acts as a lower boundary condition for land surface and hydrologic models. Shangguan et al. (2017) discussed how a constant depth to bedrock can affect model performance (e.g., Gochis et al. 2010) and outlined multiple studies which demonstrated the benefits of a dynamic depth to bedrock (e.g., Peterman et al. 2014; Brunke et al. 2016). Shangguan et al. (2017) (henceforth referred to as Shangguan) compiled global observations from soil profile data, borehole data, and remote sensing to inform a machine learning model, which resulted in global depth to bedrock estimates at a spatial resolution of 250 m. Shangguan was used in this study to determine the location of the vertical flow barrier because of its high spatial resolution and deeper bedrock estimates, up to 540 m. The dataset was mapped to a 1 km² grid over the United States

Soil data is comprised of SSURGO soils data within US borders and GSDE data for soil outside of the US. A description of the soil mapping (Schaap and Leij 1998) for this study is described in Maxwell et al. (2015). We use this soil dataset for the top 2 m (top 4 model subsurface layers) for all subsurface configuration tests. Soil data remains unchanged for the different tests. While soil parameters may influence groundwater-surface water dynamics, there is much more confidence in soil data for the United States than in the deeper subsurface. Thus, we focused on testing the data components of the deeper hydrogeology here.

Test Configurations

The tests conducted in this study are based on a tiered approach with progressive increases in complexity. Over the course of preliminary development and testing, a large number of subsurface configurations were created and used as test inputs in simulations (see SI Table 1). However, only selected configurations will be discussed here. We test four main

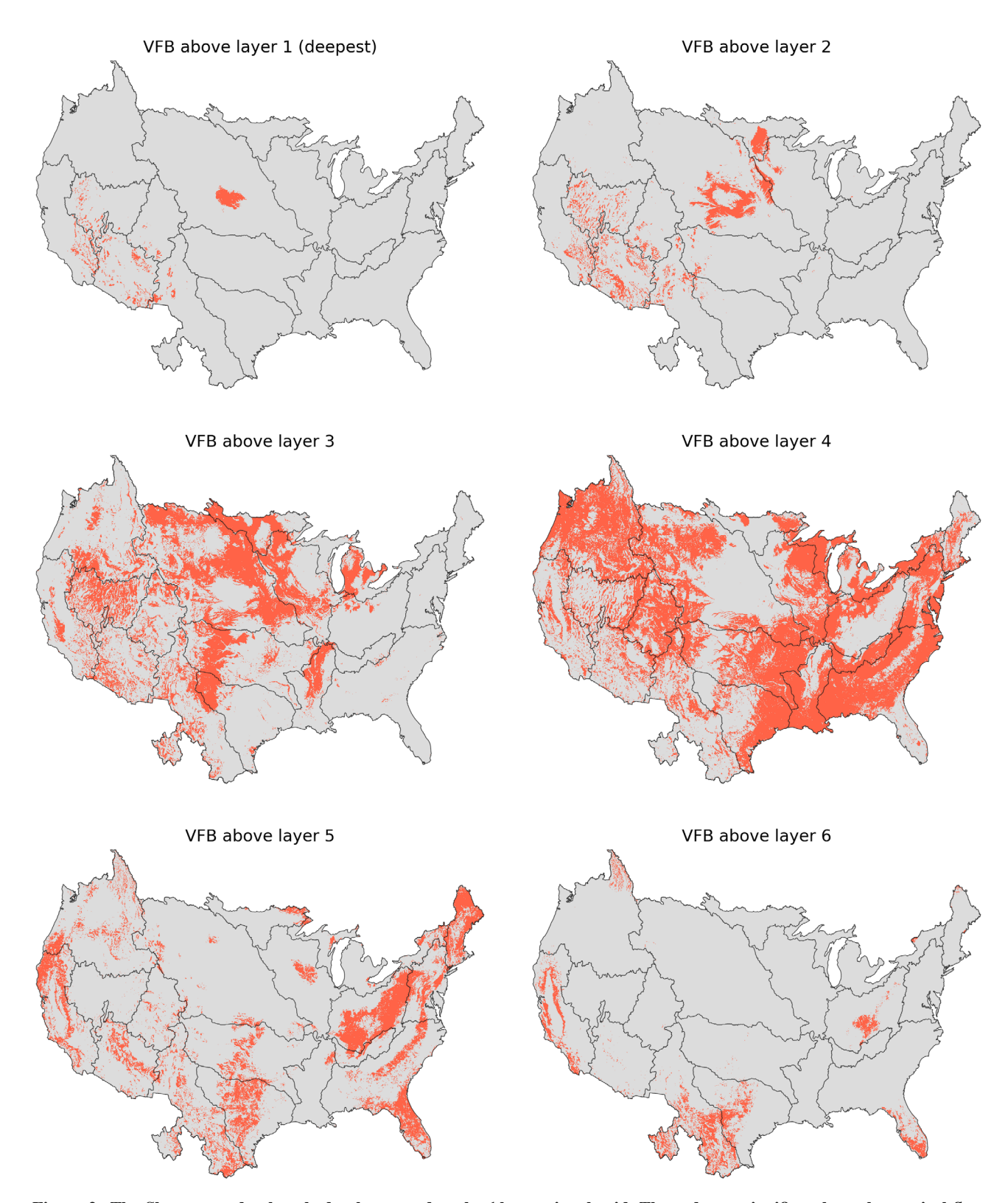


Figure 2. The Shangguan depth to bedrock mapped to the 1 km national grid. The red area signifies where the vertical flow barrier (VFB) overlays each geology model layer.

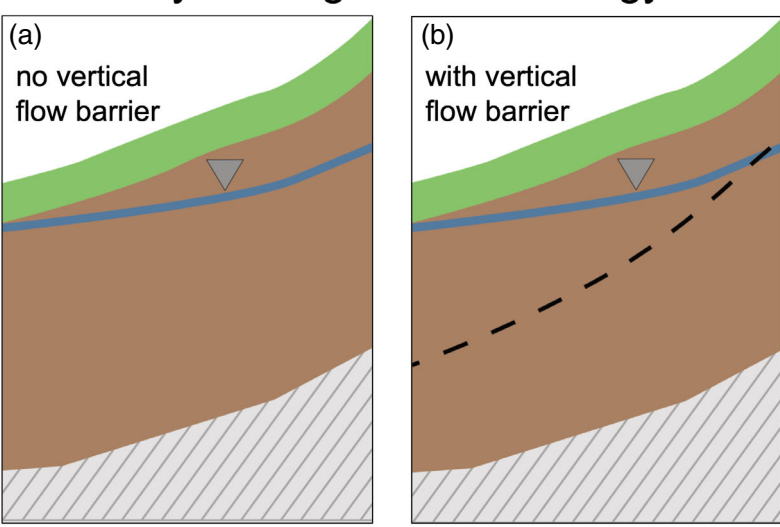
configuration types that are illustrated as conceptual models in Figure 3:

- 1 One subsurface dataset is applied as a Vertically Homogeneous geology where all 6 layers within the
- same 1 km^2 lateral grid cell contain the same geologic type (Figure 3a).
- 2 The second test type builds upon the first (1), replicating the Vertically Homogeneous geology where all 6 layers within one $1\,\mathrm{km}^2$ lateral grid cell contain the same

Table 1
Primary Tests of Main Subsurface Configurations Tested.

Test	Configuration Name	Thickness (m)	Upper Geology Dataset	Flow Barrier	Lower Geology Dataset	Anisotropy	WTD R—UCRB	WTD R—DSB	Simulated Streamflow Notes—UCRB	Simulated Streamflow Notes—DSB
-	USGS—Vertically Homogeneous	1192	USGS	None	None	None	0.87	9.0	Good match for baseflow, captures total flows closely, peak flow too	Significant overprediction of baseflow, peak flow too low
2	USGS—Simple Bedrock Layering	1192	USGS	None	USGS, bedrock set to 19	None	0.77	0.54	Significant overprediction of baseflow and total	Significant underprediction of
ϵ	USGS—Vertically Homogeneous—Constant FBz	1192	USGS	Constant 200m	None	None	Not run	0.54	now n/a	Significant underprediction of
4	USGS.—Simple Bedrock Layering.—Shangguan FBz	1192	USGS	Shangguan	USGS, bedrock set to 19	None	0.86	0.63	Baseflow matches at some locations, generally underpredicts flow. Peak	Daserlow and total flow Significant underprediction of baseflow and total flow
v	GLHYMPS 1.0—Vertically Homogeneous	1192	GLHYMPS 1.0 Single-Level	None	None	None	0.86	0.55	Significant overprediction of baseflow and total	Significant underprediction of
9	GLHYMPS 1.0—Vertically Homogeneous—Shangguan FBz	1192	GLHYMPS 1.0 Single-Level Efold	Shangguan	None	None	0.86	0.49	Baseflow matches at some locations, generally underpredicts flow. Peak	Significant of underprediction of baseflow and total flow
7	GLHYMPS 1.0—Vertically Homogeneous—Decrease	392	GLHYMPS 1.0 Single-Level	None	None	None	Not run	0.32	пом гоо сапу	Significant underprediction of
∞	GLHYMPS 2.0 over GLHYMPS 1.0—Shangguan FBz—Isotropic Geology	392	GLHYMPS 2.0	Shangguan	GLHYMPS 1.0 Single-Level Efold	None	0.71	0.12	Significant overprediction of baseflow and total flow	Significant underprediction of baseflow, flow peaks
6	GLHYMPS 2.0 over GLHYMPS 1.0—Shangguan FBz –Anisotropic Geology	392	GLHYMPS 2.0	Shangguan	GLHYMPS 1.0 Single-Level Efold	All Geology	0.71	0.15	Good match for baseflow, captures peaks and total flows closely	are better but still low Significant underprediction of baseflow, flow peaks
10	GLHYMPS 1.0—Shangguan FBz—Single E-Fold	392	GLHYMPS 1.0 Single-Level Efold	Shangguan	None	None	89.0	0.17	Good match for baseflow, captures peaks closely, total flow is high in	are better but sun low Good match for baseflow and total flow, peaks overpredicted
Ξ	GLHYMPS 1.0—Shangguan FBz—Multi E-Fold	392	GLHYMPS 1.0 Multi-Level	Shangguan	None	None	0.39	0.31	places Significant overprediction of baseflow and total	Underprediction of baseflow, flow peaks
12	GLHYMPS 1.0—Shangguan FBz—Anisotropic Selected Geology	392	GLHYMPS 1.0 Multi-Level Efold	Shangguan	None	19, 20, 21, 22, 24, 25, 26, 27	0.67	0.31	Good match for baseflow, captures peaks closely, total flow is high in places	Good match for baseflow, captures peaks and total flows closely

Vertically Homogeneous Geology



Simple Bedrock Layering

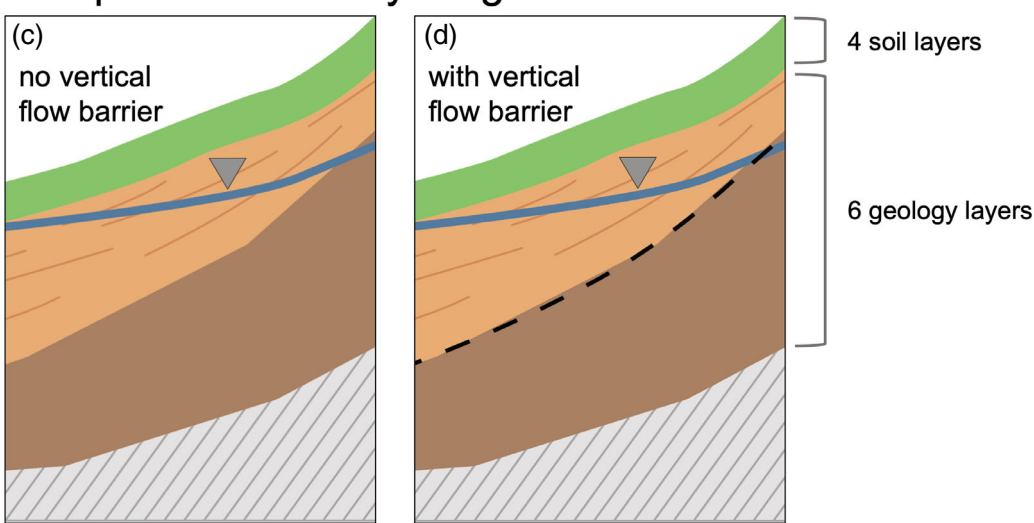


Figure 3. Diagrams depicting conceptual models of general subsurface configuration test cases. Top figures represent a Vertically Homogeneous geology layer model, omitting (a) and including (b) a vertical flow barrier. Bottom figures represent a Simple Bedrock Layering model, omitting (c) and including (d) a vertical flow barrier. Because these are conceptual diagrams, water table behavior by configuration may not be explicitly represented.

geologic type, but applies vertical flow barrier at specified depth (Figure 3b) where a vertical flux reduction is applied so that vertical flow is reduced, but not eliminated. In this approach, tests are set up to define the vertical flow barrier either at the *Shangguan* depth to bedrock or at a constant depth.

3 The third test employs a Simple Bedrock Layering technique where one geology dataset overlays a second geology dataset (Figure 3c). These two geology sets are disaggregated at the *Shangguan* bedrock depth. The goal of this layering approach is to represent unconfined and confined aquifer systems more realistically by applying a lower permeability geology at a depth where bedrock may be located.

4 The fourth test type builds upon the third (3), replicating the same Simple Bedrock Layering, but applies a vertical flow barrier (Figures 3d and 4) at the intersection of the two geology sets where a vertical flux reduction occurs so that vertical flow is reduced, but not eliminated. In this approach, tests are set up to define the vertical flow barrier at the *Shangguan* depth to bedrock.

We tested two vertical flow barriers—a constant flow barrier at a depth of 192 m and a variable depth flow barrier defined at the *Shangguan* depth to bedrock (Figures 2 and Figure S1). In both cases, a vertical flux reduction value of 0.001 (–) was assigned at the cell interface, so that the barrier maintained lateral

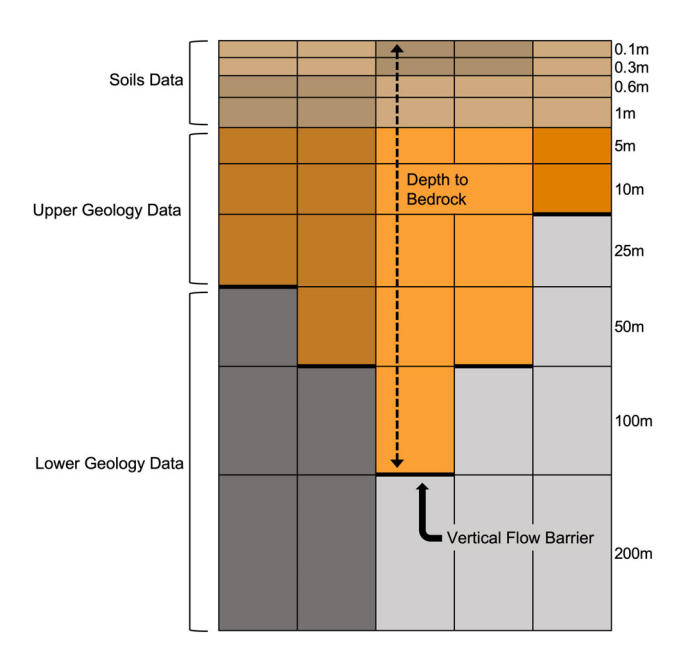


Figure 4. Conceptual model showing the upper (orange tones) and lower (gray tones) geology mapping and soils (brown tones). The vertical discretization is specific to the final subsurface dataset (figure not drawn to scale). Adapted from Swilley et al. (this issue).

flow and slowed vertical flow between model subsurface layers (Figure 4). This feature represents the boundary between the deeper confined aquifer systems and the upper unconfined aquifer systems that are dynamically connected to surface water. The configurations that use the vertical flow barrier are represented with the conceptual models in Figure 3b and 3d.

In addition to these primary test cases, we applied additional changes to configurations to test other subsurface factors. These included subsurface thickness, anisotropy changes to specified geology types, and an e-folding technique which represents the relationship between hydraulic conductivity, depth, and topography. These methods are described later in the results.

Simulations Using an Integrated Model

To test these different combinations of subsurface data, we apply each as a subsurface input file to the integrated hydrologic model ParFlow, which simultaneously solves for variably saturated groundwater flow and overland flow (Jones and Woodward 2001; Maxwell and Miller 2005; Kollet and Maxwell 2008; Maxwell 2013; Kuffour et al. 2020). ParFlow is coupled to the Common Land Model (PF-CLM), simulating hydrologic components from the bedrock to the canopy, as well as land surface energy fluxes (O'Neill et al. 2021). The integration of subsurface and surface water allows streams to form naturally at topographic convergence zones and overland flow is solved with a two-dimensional kinematic wave equation.

PF-CLM requires an indicator file consisting of subsurface inputs of distributed soil types, geologic units, and the following hydrologic properties for each subsurface unit: permeability, specific storage, porosity, and van Genuchten parameters. Subsurface properties from test datasets are vertically disaggregated and permeability indicator values are assigned to cell centers based on common geologic types. In this study, the final indicator values are based upon the continental scale model ParFlow-CONUSv1 model inputs (Maxwell et al. 2015; O'Neill et al. 2021) and are listed in the Supporting Information (Table S2). Our model has the input data requirements of a traditional land surface model (e.g., land cover, soil, and meteorological forcing) and that of a traditional groundwater model (e.g., subsurface hydrostratigraphy), thus testing these subsurface configurations with PF-CLM is relevant to other hydrologic and subsurface modeling applications which would require similar distributed data inputs. Figure 4 shows a conceptual model of the geology data within the PF-CLM gridded structure.

For this study, PF-CLM was run in two representative test subdomains (Figure 5) for each configuration at a lateral resolution of 1 km² with a 10-layer subsurface. The subsurface depth varied depending on the test configuration and was set at either 1192 m or 392 m with soil comprising the top 2 m (or the top 4 model layers) of the subsurface. The Upper Colorado River Basin (UCRB) is a 280,000 km² subdomain with complex topography which has been used in past model input testing (Tran et al. 2020). The Delaware-Susquehanna Basin (DSB) is a 103,000 km² subdomain and an area surrounding the Delaware Bay. This coastal domain possesses diverse terrain and a range of climatology, making it informative for testing subsurface properties. Both the UCRB and DSB were selected because they are part of the USGS Integrated Water Science study basins and serve as intensive regional testbeds (van Metre et al. 2020).

Each PF-CLM simulation was forced with 1 year of transient CW3E Retrospective Forcing (Pan and Lettenmaier 2023), developed from the NLDAS-2 forcing product (Xia et al. 2015a, 2015b). Each configuration was run over Water Year 2003 (October 1, 2002 to September 30, 2003). To initialize the model, each subdomain underwent a steady state spin-up, where the model was forced with potential recharge and the groundwater table was initialized; followed by a transient spin-up, where the model was forced with 2 years of the CW3E transient forcing. Through this process, a dynamic equilibration of the groundwater and surface water systems was achieved, and these resulting initial conditions were used to initialize each test simulation. It is also important to note that these simulations are considered predevelopment, in that they do not account for anthropogenic influences such as irrigation, groundwater pumping, or dams. Simulations were conducted on the NCAR Cheyenne high performance computing system (Computational and Information Systems Laboratory 2019).

Model Evaluation

To understand how each subsurface configuration performs in a PF-CLM simulation, we examine both

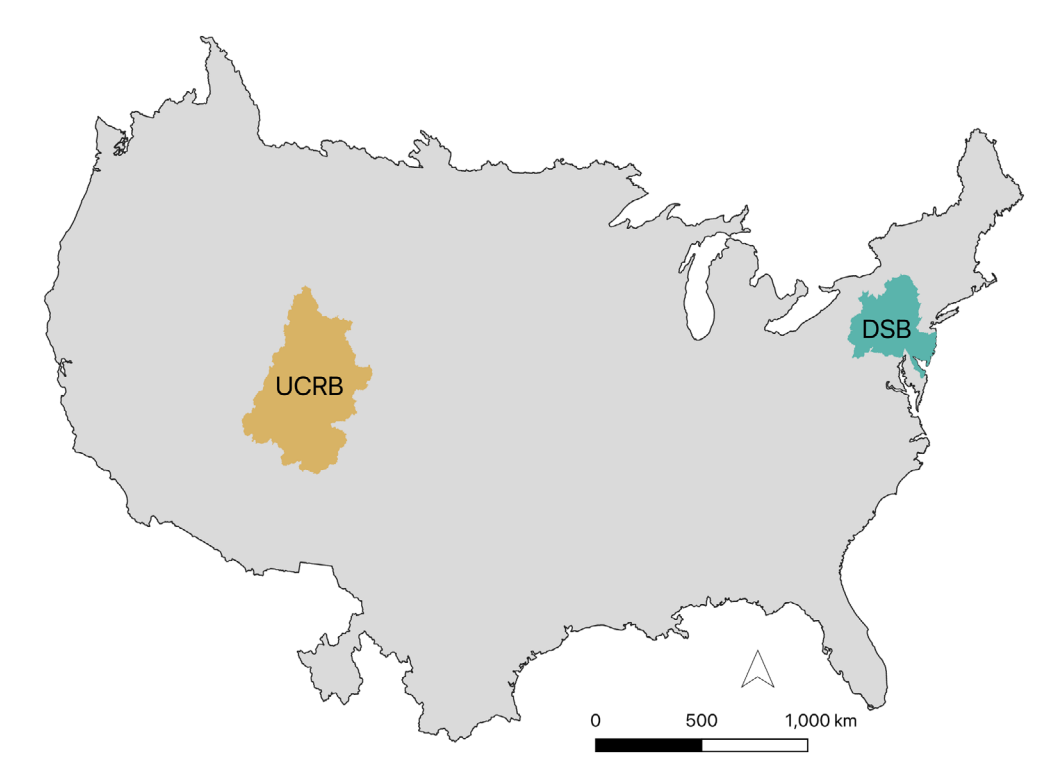


Figure 5. The inset maps show the Upper Colorado River Basin (brown) and Delaware-Susquehanna Basin (green) model test domains. The gray map of the CONUS shows the extent of the final dataset.

spatial groundwater behavior and streamflow dynamics. Annual average PF-CLM water table depth (WTD) was compared to long term, steady state WTD observations from (Fan et al. 2007, 2013). For the United States, Fan et al. collected water table observations from over 500,000 sites between 1927 and 2009. This dataset was used to evaluate long-term, steady-state PF-CLM annual averaged WTD for the different subsurface configuration runs in each subdomain. A Pearson correlation coefficient (R) was calculated for each subsurface configuration to determine general groundwater performance in each subdomain. To evaluate streamflow, we compared daily streamflow from PF-CLM to observations from USGS gages. Modeled versus observed hydrographs were visually inspected to determine general streamflow performance, particularly to observe baseflow dynamics.

Even with a seemingly comprehensive number of streamflow and groundwater observations, the evaluation of model performance was still a mix of a quantitative and qualitative evaluation. WTD observations are sparse in time and were used to evaluate spatial configuration, streamflow was used to evaluate temporal performance. While additional measures may be important in some circumstances, these two measures were chosen because they provide insight into many, if not all, aspects of the hydrologic system.

It was important for this study to analyze results of both steady-state WTD and temporal streamflow dynamics to better understand general groundwater behavior and watershed response from varying the hydrogeologic input dataset. In considering steady state WTD, we observe spatial groundwater patterns, which are influenced by geology and hydrogeology factors. Streamflow timeseries are important to show watershed response to the hydrostratigraphy data, particularly the groundwater-surface water interactions, such as baseflow. This approach informs how different subsurface configurations compare to each other and how each may affect model output.

Results

Over the broad duration of this study, over 80 different configurations were tested (Table S1). These simulations produced an immense volume of information and data and many were very poor performing (e.g., Figure S4). As such, we will only present results from the primary datasets and the most pertinent subsurface configurations that represent examples from the four main test types (Figure 3) and highlight model performance. Table 1 shows the primary 12 runs. These configurations represent the core datasets (i.e., GLHYMPS 1.0, GLHYMPS 2.0, USGS, Shangguan depth to bedrock) and the main subsurface components from Figure 1 (i.e., bedrock representation, vertical flow barrier, effective subsurface thickness, and anisotropy). The table describes which dataset was used for the upper and lower geology, if a depth to bedrock was applied, and lists WTD statistics and qualitative streamflow notes for both UCRB and DSB subdomains. A full description of each configuration and a complete list of all configurations tested can be found in the Supplementary Information (Text S1).

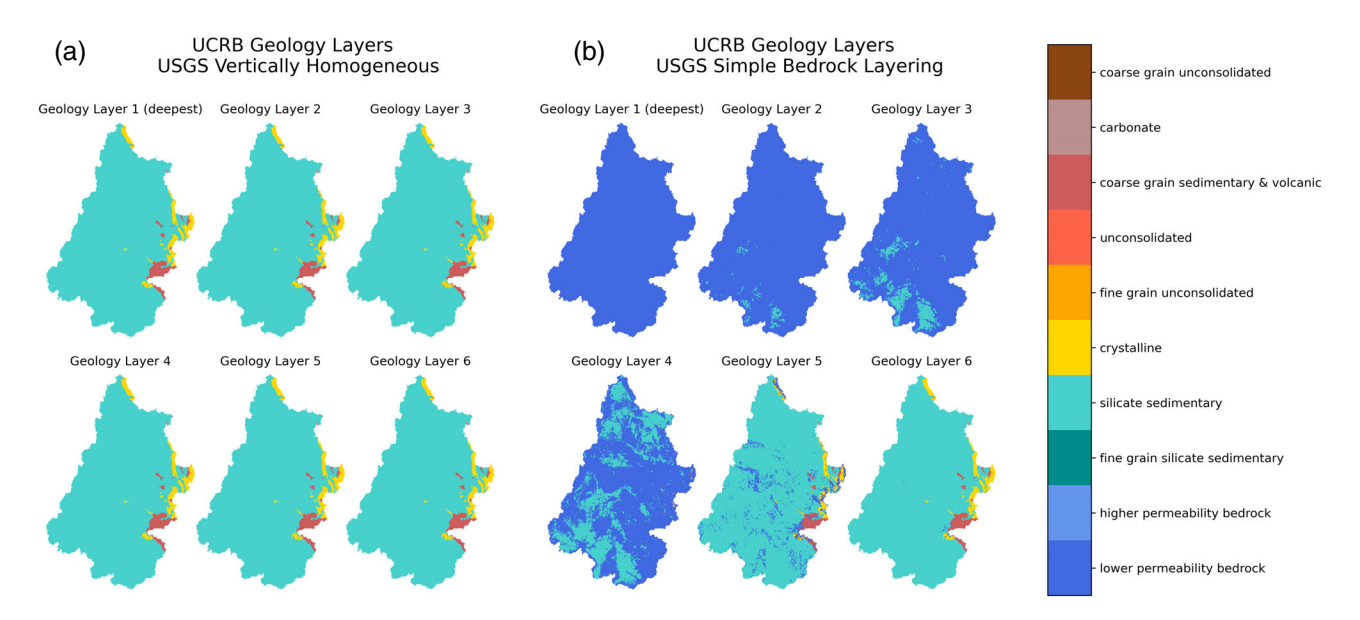


Figure 6. Maps of the UCRB subdomain geology layers for the (a) USGS Vertically Homogeneous (*Test 1*) and (b) USGS Simple Bedrock Layering (*Test 2*) configurations. Colors represent geology indicator values. Note that Geology Layer 1 signifies the deepest subsurface layer.

Vertically Homogeneous and Simple Bedrock Layering Configurations

The results here focus on the PF-CLM simulations from the UCRB and DSB subdomains. As mentioned in the methods, our tests are based on a tiered approach starting with a Vertically Homogeneous, distributed subsurface. Bedrock is an important boundary in hydrologic modeling so one of the first components to test was whether a Simple Bedrock Layering approach (Figure 3c) is an improvement to a Vertically Homogeneous geology (Figure 3a).

Test 1 and Test 2 from Table 1 are examples of this. Both tests use the USGS combined Primary Aquifer and Secondary Hydrogeologic Region dataset. Test 1 (Figure 6a) represents the Vertically Homogeneous subsurface with all 6 geologic layers identified with the same indicator, resulting in the same geologic type below the soil at each 1 km lateral grid cell. Alternatively, Test 2 (Figure 6b) uses the same USGS dataset but imposes bedrock layering occurring at the depth of Shangguan with a constant, low permeability bedrock with a hydraulic conductivity of 0.005 m/h (PF-CONUS indicator 19, Table S2).

Results show that overall, both the Vertically Homogeneous (*Test 1*) and Simple Bedrock Layering (*Test 2*) configurations have promising WTD correlations for the UCRB (*R* correlation of 0.87 and 0.77, respectively) and DSB (*R* correlation of 0.65 and 0.54, respectively). However, when inspecting hydrographs (Figure 7), baseflow for the DSB Vertically Homogeneous case is either significantly over- or underpredicted except (*Test 1*, Figure 7a and 7b). This is an interesting result that demonstrates how evaluating model results for both water table depth and streamflow limit the overall parameter space. That is, while multiple subsurface

models may exhibit equally good match to water table depth, these subsurface architectures do not all produce the same streamflow response as hydraulic conductivity values will partition water differently into changes in streamflow and subsurface storage with time (Foster and Maxwell 2019). Given that higher hydraulic conductivity values increase the baseflow response and decrease peak flows, particularly in snowmelt dominated systems like the UCRB, the ability of different configurations to match the base and peak flows provides an important control on the subsurface configuration.

Vertical Flow Barrier

DSB Test 3 and Test 4 are examples of adding in a flow barrier along with the USGS geology dataset. Test 3 applies a constant flow barrier set at a depth of 192 m or just above the deepest model subsurface layer. The average WTD correlation was 0.54, the same as the DSB USGS Simple Bedrock Layering (Test 2). The constant flow barrier (Test 3) did not improve model performance for either WTD or streamflow, with at nearly all gages underpredicting flow. However, when a variable depth flow barrier based on Shangguan depth to bedrock was applied (Test 4) there are significant improvements in performance (Figure 8). The average WTD correlation in DSB for Test 4 was 0.63 and baseflow and peak flows closely match observations.

Improvements with a vertical flow barrier are also seen for the UCRB subdomain in tests that use the *GLHYMPS 1.0* Vertically Homogeneous configuration omitting (*Test 5*) and adding (*Test 6*) the *Shangguan* flow barrier especially in the UCRB domain (Figure 9). These tests both have the same WTD correlation of 0.86, but there are dramatic differences in baseflow—without the flow barrier applied, baseflow

USGS – vertically homogeneous (*Test 1*) USGS – simple bedrock layering (*Test 2*)

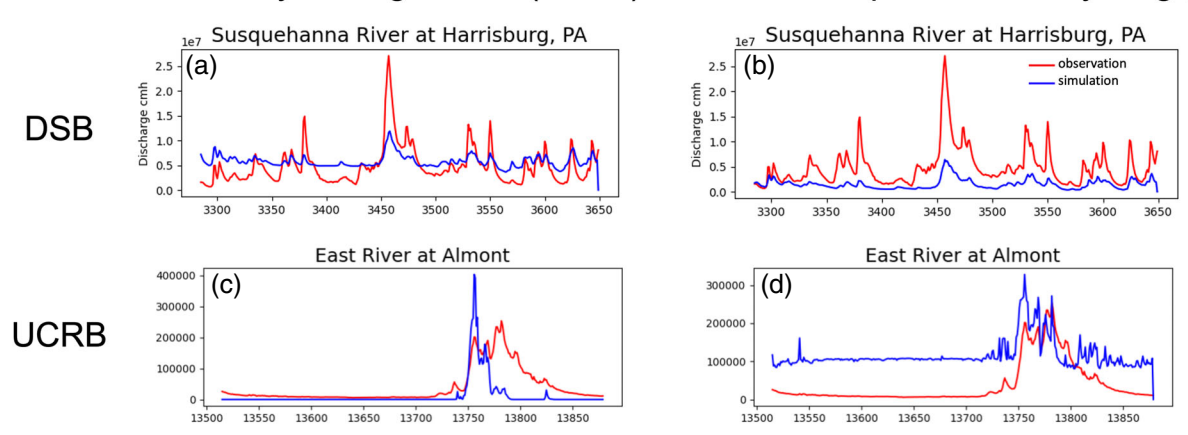


Figure 7. Examples of streamflow for the USGS Vertically Homogeneous configuration *Test 1* (a, c) and USGS Simple Bedrock Layering configuration *Test 2* (b, d). Red lines indicate observations and blue lines indicate simulations. Streamflow is in cubic meters per hour.



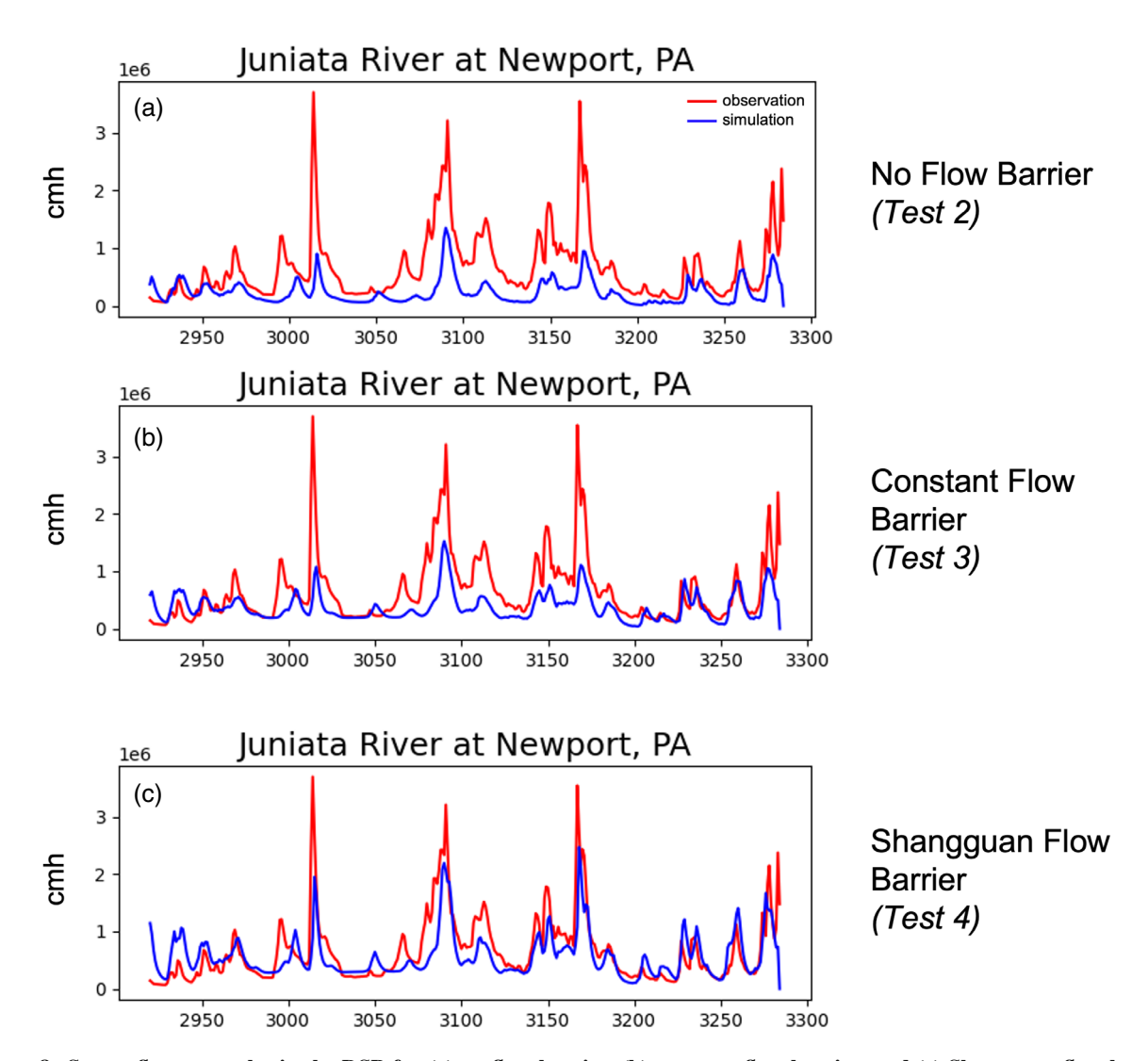
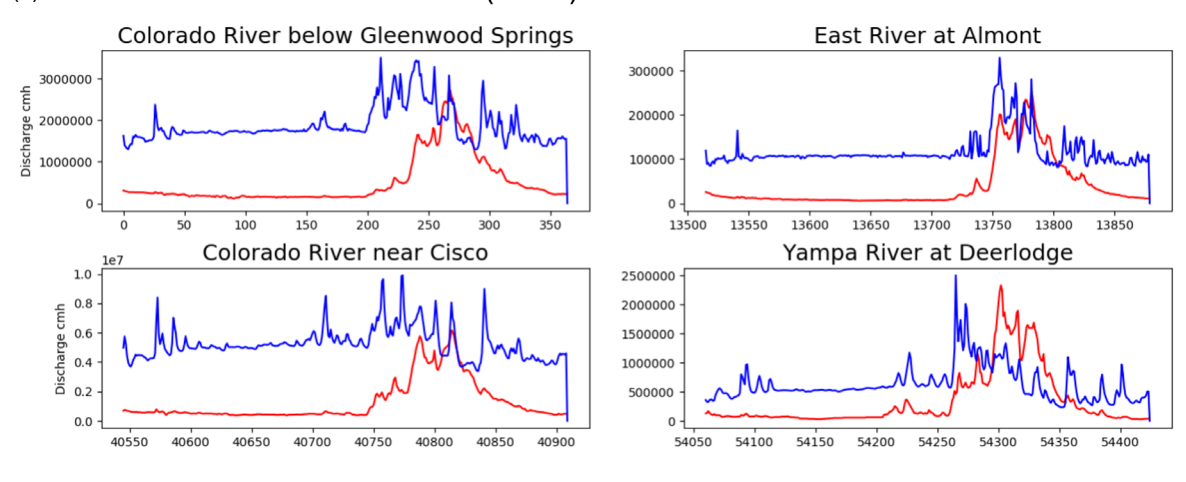


Figure 8. Streamflow examples in the DSB for (a) no flow barrier, (b) constant flow barrier, and (c) Shangguan flow barrier. Red lines indicate observations and blue lines indicate simulations. Streamflow is in cubic meters per hour.

(a) UCRB without a vertical flow barrier (Test 5)



(b) UCRB with a vertical flow barrier at the Shangguan depth to bedrock (Test 6)

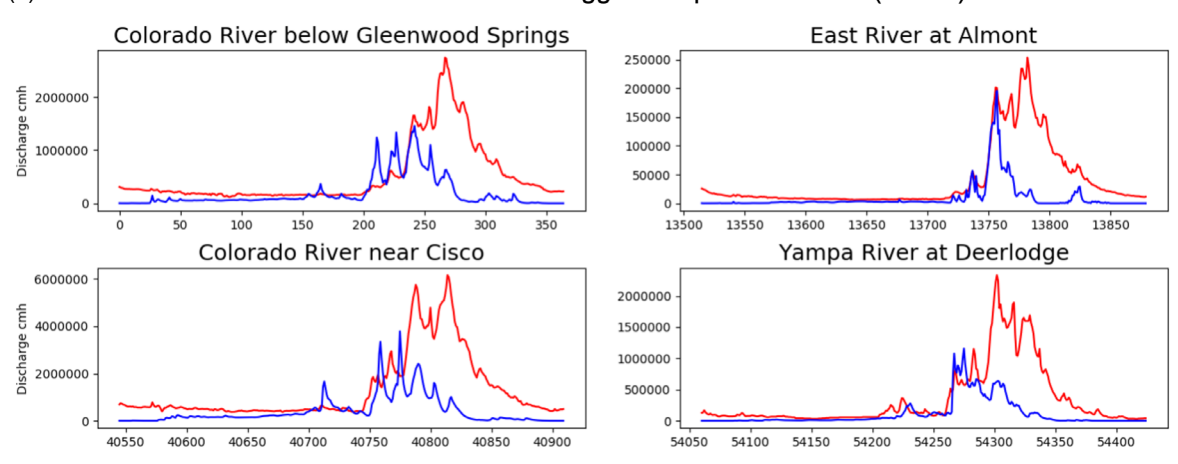


Figure 9. Streamflow examples in the UCRB for (a) no flow barrier ($Test\ 5$) and (b) Shangguan flow barrier ($Test\ 6$) for the GLHYMPS 1.0 Vertically Homogeneous configuration. Red lines indicate observations and blue lines indicate simulations. Streamflow is in cubic meters per hour.

is significantly overpredicted. High baseflow and lower peaks are also exhibited in the UCRB (Figure 7d), with the Simple Bedrock Layering and without a vertical flow barrier. These tests emphasize the importance of groundwater-surface water interactions and show that even if the depth to water table remains the same, the contribution to streamflow differs greatly.

This further highlights the discussion for *Test 1* and *Test 2*, above, that multiple constraints provide better evaluation of subsurface datasets. Given the dependence of baseflow on overall transmissivity of the system; the flow barrier acts to reduce transmissivity of the system which lowers baseflow. This is in contrast with changes in overall subsurface depth or an impermeable bedrock (e.g., Figure 3a) as this allows for simulation of an aquifer system that is in more direct contact with streamflow and land surface processes, and a confined aquifer system that is somewhat removed from the surface flow, but still present and connected. Representation of both of these systems was considered important given that often groundwater extraction may occur from such a lower, confined system.

Additional Tests

To evaluate the influence of other subsurface factors, additional tests were run to supplement the main test configurations. These included subsurface thickness, anisotropy changes to specified geology types, and an e-folding technique.

The depth of the PF-CLM model, or subsurface thickness, was another consideration for how we represent aquifer systems in each configuration. Gleeson et al. (2016) showed that circulated groundwater is commonly found at depths up to 250 m and Mcintosh et al. (2012) found Late Pleistocene recharge reach up to 1000 m in sedimentary basins. Condon et al. (2020) suggests that modelers should critically assess if "deep" flow paths are relevant to a study area. Since our goal is to generate a subsurface configuration for the entire CONUS, it is likely that there are locations where deep flow paths contribute to streamflow or a catchment water balance, even if this is not the case across the entire continent. Therefore, we conducted tests where a flow barrier was applied and changed the total subsurface thickness to either 1192 m or 392 m, which essentially changes

the depth of the represented unconfined aquifer. This test builds on the results of Swilley et al. (this issue) that tested only a 1192 m total model thickness for the UCRB.

One main consideration for reducing the subsurface thickness has to do with the systematic biases on transmissivity that result from vertical model resolution and effective hydraulic conductivity. For example, the 1192 m deep, 10-layer subsurface has a bottom layer that is 1000 m thick. If we apply a bedrock hydraulic conductivity of 0.005 m/h, this results in a transmissivity of 5 m²/h. Then consider the 392 m deep, 10-layer subsurface has a bottom layer that is 200 m thick. If that same bedrock hydraulic conductivity of 0.005 m/h is applied, the transmissivity is 1 m²/h. Therefore, with the deeper, thicker subsurface configuration, the bedrock is five times more transmissive than the shallower configuration. This has implications on the surface water partitioning and the amount of baseflow present. Swilley et al. (this issue) shows that both adding a vertical flow barrier and reducing the subsurface model layer thickness reduces the effective transmissivity and reduces groundwater driven baseflow to streams in the UCRB. This is consistent with findings in Foster and Maxwell (2019) where higher hydraulic conductivity values resulted in increased baseflow discharge because of the high subsurface flow rate.

The DSB subdomain exhibits low baseflow in nearly all primary tests. Decreasing the thickness of the subsurface results in increased base flow and peaks that more closely match observations. *Test 5* and *Test 7* in the DSB use the same *GLHYMPS 1.0* base dataset and have an overall thickness of 1192 and 392 m, respectively. Decreasing the thickness leads to worse WTD correlation, but better baseflow matches. More indicative are the tests where the vertical flow barrier is added (*Test 2* and *Test 4*, Figure 8). Adding a flow barrier improves simulation results, particularly streamflow. Swilley et al. (this issue) discuss that the addition of the flow barrier decreases the effective subsurface thickness and illustrates the groundwater-surface water interactions.

The representation of anisotropy can have a significant impact on groundwater modeling and groundwater-surface water interactions (Borghi et al. 2015). We conducted many tests to better understand whether anisotropy would impact model results in the two test subdomains (Table S1). Our method of applying anisotropy is as a tensor value in the z direction for certain geologic units, reducing it by a factor of 0.1 (with 1.0 in the x and y direction; see the *ParFlow user's manual* (Maxwell et al. 2023). Physically, this reduces the vertical saturated hydraulic conductivity which limits flow perpendicular to the topography and leaves the horizontal values unchanged.

Our results show compelling arguments for including anisotropy as an additional methodology to the specified subsurface data. For example, UCRB *Test 8* and *Test 9* (*GLHYMPS 2.0* over *GLHYMPS 1.0*, *Shangguan* flow barrier) differ in that *Test 8* applies isotropic geology and

Test 9 applies anisotropic geology. Both Test 8 and Test 9 have a WTD correlation of 0.71, but there is a significant reduction and improvement to baseflow representation with the addition of anisotropy in Test 9 (Figure 10). Similarly, adding anisotropy in Test 12, compared to the same configuration in Test 11 (GLHYMPS 1.0, Shangguan flow barrier) shows significant improvements in baseflow for both UCRB and DSB and improvements to WTD for UCRB with R correlations of 0.39 and 0.67 for Test 11 and Test 12, respectively (DSB WTD R correlation was 0.31 for both Test 11 and Test 12) (Table 1).

While there is theoretical discussion of decreasing

hydraulic conductivity with depth, relatively few studies

have explored potential impacts at regional scales (e.g.,

Belcher et al. 2001; Fan et al. 2007; Jiang et al. 2009). Belcher et al. (2001) compiled a substantial number of aquifer tests and found a noisy relationship between depth and hydraulic conductivity. We also explored a relationship between hydraulic conductivity and slope, to reflect the effects of topography by an e-folding relationship derived by Fan et al. (2007) and instantiated by Maxwell et al. (2015) $\exp\left(-\frac{z}{f}\right)$, where z is the depth below-ground surface in meters calculated at the midpoint of a grid cell and $f = \frac{a}{1 + b\sqrt{S_x^2 + S_y^2}}$, where $S_{x,y}$ are the topographic slopes in the x, y direction, a = 20, and b = 125. The application of this relationship decreases the hydraulic conductivity of the bottom layer with depth and at places of steep topography. Simulations were conducted that reduced the hydraulic conductivity as a function of slope alone (a constant z, Single E-fold shown in Figure 11a) compared to a decrease in conductivity with depth (Multi E-fold shown in Figure 11b).

Results show (Table 1) that for all *USGS* and most *GLHYMPS* test configurations (*Tests 1 to 9*), simulated streamflow in the DSB was significantly underpredicted (except for overprediction in *Test 1*). For the single e-folding *GLHYMPS 1.0* test with a vertical flow barrier (*Test 10*, Figure 11a), streamflow in the DSB improved significantly, however WTD correlation was only 0.17. Introducing the *GLHYMPS 1.0* multi e-folding (*Test 11*, Figure 11b), increased DSB WTD correlation to 0.31.

Selected National Configuration

For this study, we present a Selected National Configuration which most reasonably represents the whole of the continental United States (Figure 12) and builds upon the components discussed in the results thus far. The Selected National Configuration consists of *GLHYMPS 1.0* for both upper and lower geologies, the *Shangguan* depth to bedrock dataset for a vertical flow barrier, anisotropy applied to specified geology types (excluding sand, coarse grained unconsolidated material, and karst aquifer materials); and implementation of multi-level e-folding (Table 1, *Test 12*). It has a lateral resolution of 1 km², a depth of 392 m, and consists of 10 vertical layers disaggregated between soil (top four layers) and geology (lower six layers).

UCRB Test 8 (top), Test 9 (bottom) - GLHYMPS 2.0 upper, GLHYMPS 1.0 lower, 392m, Shangguan FB

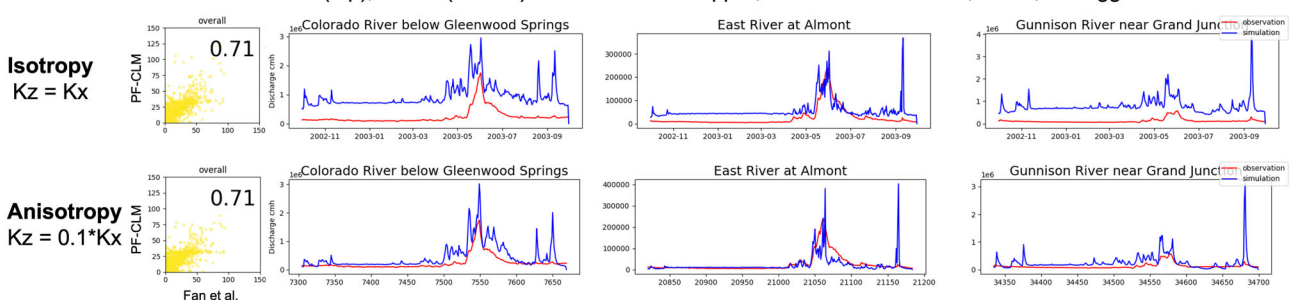


Figure 10. Examples showing compared WTD and streamflow for configurations applying isotropy and anisotropy to selected geologic types. Each run uses GLHYMPS 2.0 upper, GLHYMPS 1.0 lower, 392 m depth, and Shangguan flow barrier. Red lines indicate observations and blue lines indicate simulations.

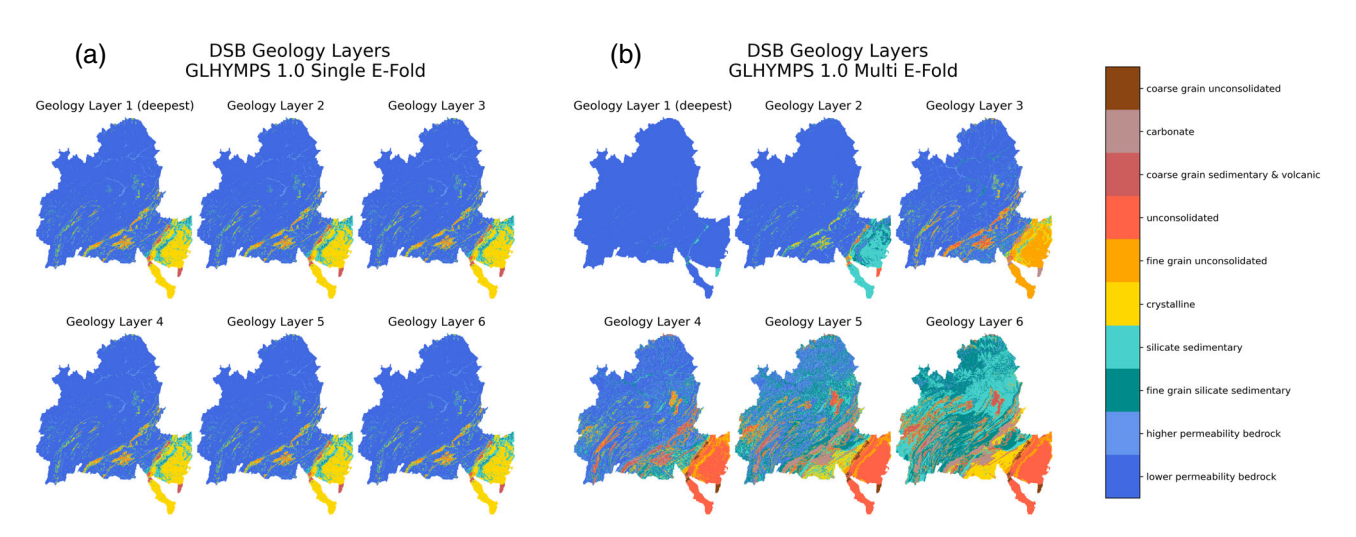


Figure 11. Comparison of (a) single-layer e-folding and (b) multilayer e-folding for the DSB subdomain. Colors represent different geologic indicators and Geology Layer 1 is the deepest layer.

Ultimately, the Selected National Configuration was chosen based on streamflow and WTD performance in both the UCRB and DSB subdomain. This configuration had WTD correlation in the UCRB (0.67) and DSB (0.31), which is a much more stringent performance metric than hydraulic head (e.g., Maxwell et al. 2015; Reinecke et al. 2020) and, compared to the evaluation of many large-scale simulations of WTD (Reinecke et al. 2020, Figure 7), the performance shown here is a favorable improvement over prior large-scale studies. Additionally, hydrographs reveal that baseflow, flow peaks, and flow volume are well represented for both subdomains (Figure 13b and 13d).

Two other configurations performed comparably to the Selected National Configuration: the *USGS* Vertically Homogeneous configuration (*Test 1*) and the *USGS* Simple Bedrock Layering with the vertical flow barrier at *Shangguan* depth to bedrock (*Test 4*). *Test 1* had the best combined WTD correlation for both subdomains (0.87 for UCRB and 0.65 for DSB), but when also taking streamflow into account, this configuration tended to either over- or underpredict baseflow and total flow in both subdomains. For example, the *Test 1* configuration

significantly overpredicted baseflow and underpredicted flow peaks in the DSB (Figure 7a and S2). *Test 4* also had favorable WTD (0.86 for UCRB and 0.63 for DSB), but again, considering streamflow dynamics, baseflow and peak flow were underpredicted in both the UCRB and DSB (Figure S3). These configurations highlight baseflow and peak flow sensitivity to differing hydraulic conductivities, also exemplified in Figures 8 and 9.

Resolution and extent of the data products was a secondary deciding factor. *GLHYMPS 1.0* is higher resolution than *USGS*—the average polygon size for the *USGS* Secondary Hydrogeologic Regions is approximately 46,000 km² (Belitz et al. 2019), compared to a polygon size for *GLHYMPS 1.0* of approximately 100 km² (Gleeson et al. 2014). Additionally, the *USGS* Primary Aquifer and Secondary Hydrogeologic Region mapping is limited to the contiguous U.S. boundary. *GLHYMPS* being a global dataset, includes data outside of the United States. This is important for continuity in subsurface data across political boundaries, for example, continental scale modeling applications that include transboundary watersheds extending into Mexico and Canada (see Figure 12 boundaries).

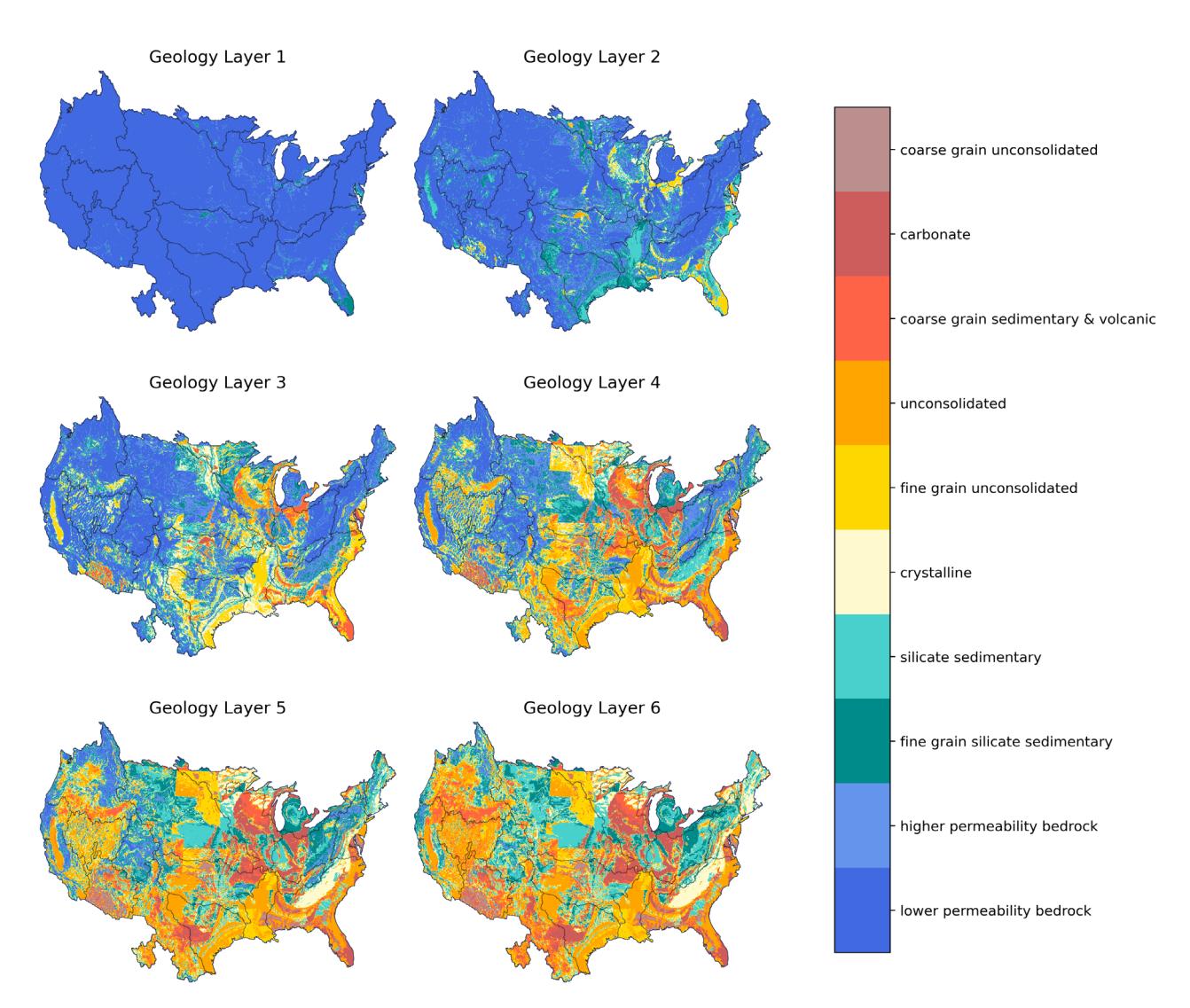


Figure 12. The selected national configuration (GLHYMPS1.0, Shangguan flow barrier, 392 m, multilevel e-folding, anisotropy) for the entire CONUS at 1 km resolution. Colors indicate different geologic types representing the geologic indicators in PF-CLM. Geology Layer 1 is the deepest layer.

One of the advantages to the methods in this study is that both WTD and streamflow were accounted for in each configuration test. While some of the configurations had higher correlation between modeled and observed WTD, many of these had very poor performing streamflow. Thus, the final configuration was selected to capture overall performance regarding groundwater-surface water interactions. For these reasons, we determine that the *USGS* configurations *Test 1* and *Test 4* may be good alternative datasets depending on the region, but that the Selected National Configuration is the optimal dataset for the CONUS. These results emphasize the challenges of developing a seamless and conceptually consistent dataset over the continent, in contrast to developing discrete, small-scale calibrated models.

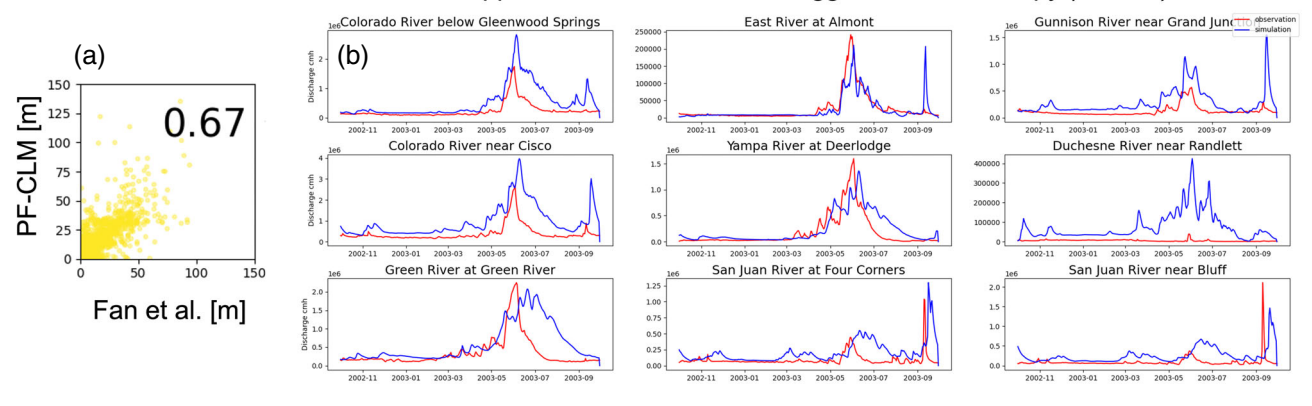
The data for the Selected National Configuration, as well as the other primary configurations discussed in the results are publicly available via HydroFrame (hydroframe.org) and the Princeton Hydrologic Data Center (PHDC).

Conclusions

We present a systematic analysis for testing continental scale subsurface datasets for use in hydrological modeling. We evaluated a range of configurations compiled from available subsurface datasets using an integrated hydrologic model. We compared simulation results to observations to evaluate the performance of each subsurface configuration on groundwater-surface water interactions.

Our main findings show that the thickness of the subsurface is important for representing the connectivity between groundwater and surface water. Drawing upon the conceptual models shown in Figure 3, we can draw some general conclusions from this work. Vertical homogeneity (Figure 3a and 3b) results in too large a lateral transmissivity for reasonable domain thicknesses. This results in very large flows, especially baseflows. The addition of the vertical flow barrier, or confining unit (Figure 3b and 3d) limits the overall transmissivity of the subsurface that is in contact with the stream network

UCRB - GLHYMPS 1.0 upper and lower, 392m, Shangguan FB, anisotropy (Test 12)



DSB – GLHYMPS 1.0 upper and lower, 392m, Shangguan FB, anisotropy (Test 12)

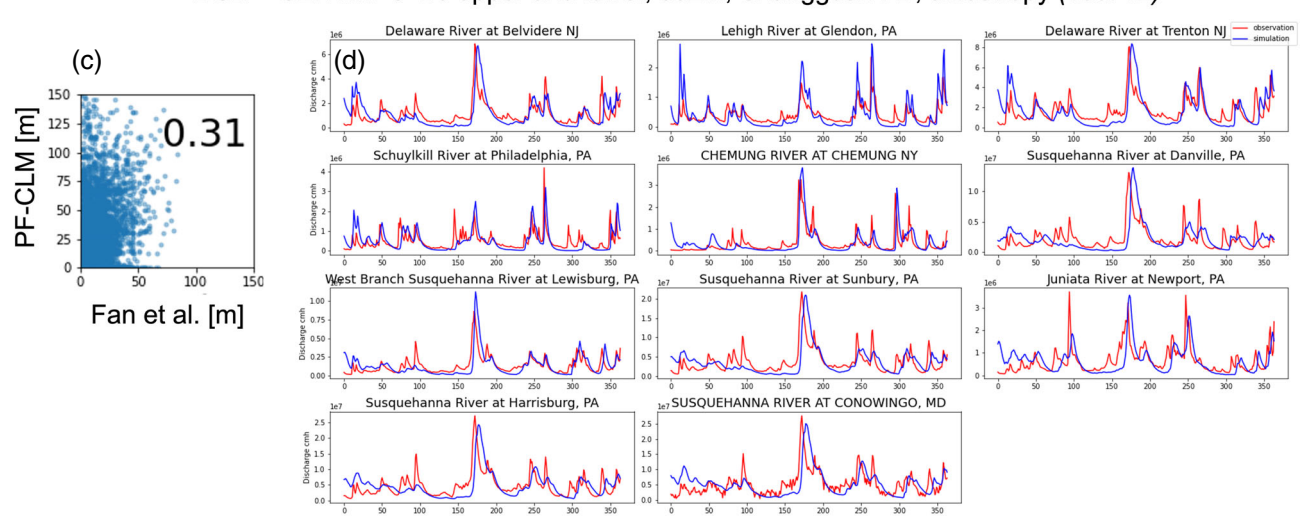


Figure 13. Evaluation of WTD and streamflow in the UCRB (a, b) and the DSB subdomain (c, d) for the Selected National Configuration dataset.

and reduces baseflow and increases streamflow response to precipitation events. The three-dimensional bedrock layering improves the fidelity of spatial groundwater distribution (Figure 3c and 3d) but without the confining layer still results in baseflow that is too large. Therefore, we find that the configurations that include a vertical flow barrier, and thus decrease the overall thickness, significantly improve simulation results, particularly for baseflow. Moreover, we find that while groundwater simulation may be a focal point for using these datasets, it is vital to also observe the performance of simulated streamflow and consider surface water and groundwater partitioning.

Additionally, changes in subsurface configuration will also shift the overall water balance in the basin. In our simulations, precipitation (i.e., basin inflow) is the same across all cases and the changes in storage are minimal. Therefore, the primary changes we expect to see are shifts between the relative importance of ET and streamflow. Increasing K with depth tends to increase base flow and total streamflow. Conversely, higher overall K values are generally correlated with deeper water table depths and decreased ET (suggested by Kollet and Maxwell 2008,

among others). Consistent with these trends, in our simulations the average K values range from 0.0172 to 0.0321 m/h for the DSB and 0.0150 to 0.0249 m/h for the UCRB. We see generally higher streamflow in the highest K case and lower streamflow in the lowest K case.

We have settled on a Selected National Configuration, which we have highlighted and results in good overall model performance when considering both WTD and streamflow in the two test subdomains. However, the *USGS* configuration also had favorable results for WTD and could be used as an alternate model. The Selected National Configuration dataset is publicly available and can be used in a range of hydrologic and hydrogeologic modeling applications.

The overarching goals of this study were to increase understanding of how subsurface permeability characterization impacts hydrologic model results and to compile a nationally consistent hydrostratigraphy dataset from existing subsurface datasets for use in continental-scale hydrological modeling applications. While testing multiple subsurface configurations using a national-scale model remains computationally expensive and generally unfeasible, testing in smaller subdomains enabled

many subsurface cases to be implemented and evaluated. As a next step, we plan to test the Selected National Configuration at the national scale as a subsurface input to the updated ParFlow-CONUSv2 continental-scale hydrological model. The results of this simulation will provide more information about large-scale performance and areas of potential improvement.

Defining large-scale geology accurately is a very challenging problem and our goal is to find an optimal dataset for the entire CONUS. We fully recognize that this is a work in progress and that there is always room for development as new data emerge and methodologies progress for characterizing the subsurface. This is a snapshot of the work as we evolve better hydrology models of the United States.

Acknowledgments

This research has been supported by the U.S. Department of Energy Office of Science (DE-AC02-05CH11231) and the U.S. National Science Foundation Office of Advanced Cyberinfrastructure (OAC-2054506 and OAC-1835855). The authors acknowledge the NCAR CISL Cheyenne supercomputing resources made available for conducting simulations and model postprocessing for this study (doi:10.5065/D6RX99HX). Data products will be made available via the HydroFrame project (https://hydroframe.org) upon final publication. We thank the Editor in Chief (L. Konikow), Executive Editor (M. Hill), and two anonymous reviewers for their constructive comments which have added to the quality and clarity of this work.

Authors' Note

The authors declare no conflict of interest.

Supporting Information

Additional supporting information may be found online in the Supporting Information section at the end of the article. Supporting Information is generally *not* peer reviewed.

- Data S1. Test subsurface configuration descriptions.
- Text S2. Meteorological forcing.
- **Figure S1.** *Shangguan* depth to bedrock for the (a) DSB and (b) UCRB subdomains.
- **Figure S2.** The results for the *USGS* Vertically Homogeneous configuration (*Test 1*). Considered an alternative approach to the Selected National Configuration.
- **Figure S3.** The results for the *USGS* Simple Bedrock Layering configuration with vertical flow barrier at *Shangguan (Test 4)*. Considered an alternative approach to the Selected National Configuration.
- **Figure S4.** An example of a poor performing configuration that was not included in the manuscript comparison. **Table S1.** All subsurface test configurations run with PF-CLM.

- **Table S2.** PF-CLM soil and subsurface geology indicator permeability values.
- **Table S3.** PF-CLM subsurface indicators where anisotropy was applied for Selected National Configuration.

References

- Abimbola, O.P., A.R. Mittelstet, T.E. Gilmore, and J.T. Korus. 2020. Influence of watershed characteristics on streambed hydraulic conductivity across multiple stream orders. *Scientific Reports* 10, no. 1: 3696. https://doi.org/10.1038/s41598-020-60658-3
- Araya, S.N., and T.A. Ghezzehei. 2019. Using machine learning for prediction of saturated hydraulic conductivity and its sensitivity to soil structural perturbations. *Water Resources Research* 55, no. 7: 5715–5737. https://doi.org/10.1029/2018WR024357
- Back, W., J.S. Rosenshein, and P.R. Seaber. 1988. In *Hydrogeology*, ed. William Back, Joseph S. Rosenshein, and Paul R. Seaber. Boulder, Colorado: Geological Society of America.
- Belcher, W. R., P. E. Elliott, and A. L. Geldon. 2001. Hydraulic-property estimates for use with a transient ground-water flow model of the death valley regional ground-water flow system, Nevada and California. U.S. Geol. Survey Water-Resources Investigations Report 01-4210. https://pubs.usgs.gov/wri/wri014210/book/wri014210.pdf.
- Belitz, K., E. Watson, T.D. Johnson, and J. Sharpe. 2019. Secondary hydrogeologic regions of the conterminous United States. *Groundwater* 57, no. 3: 367–377. https://doi.org/10.1111/gwat.12806
- Borghi, A., P. Renard, and G. Courrioux. 2015. Generation of 3D spatially variable anisotropy for groundwater flow simulations. *Groundwater* 53, no. 6: 955–958. https://doi.org/10.1111/gwat.12295
- Brunke, M.A., P. Broxton, J. Pelletier, D. Gochis, P. Hazenberg, D.M. Lawrence, L.R. Leung, G.-Y. Niu, P.A. Troch, and X. Zeng. 2016. Implementing and evaluating variable soil thickness in the community land model, version 4.5 (CLM4.5). *Journal of Climate* 29, no. 9: 3441–3461. https://doi.org/10.1175/JCLI-D-15-0307.s1
- Chaney, N.W., B. Minasny, J.D. Herman, T.W. Nauman, C.W. Brungard, C.L.S. Morgan, A.B. McBratney, E.F. Wood, and Y. Yimam. 2019. POLARIS soil properties: 30-m probabilistic maps of soil properties over the contiguous United States. *Water Resources Research* 55, no. 4: 2916–2938. https://doi.org/10.1029/2018WR022797
- Computational and Information Systems Laboratory. 2019. Cheyenne: HPE/SGI ICE XA System (University Community Computing). Boulder, Colorado: National Center for Atmospheric Research. https://doi.org/10.5065/D6RX99HX
- Condon, L.E., S. Kollet, M.F.P. Bierkens, G.E. Fogg, R.M. Maxwell, M.C. Hill, H.H. Fransen, A. Verhoef, A.F. Van Loon, M. Sulis, and C. Abesser. 2021. Global groundwater modeling and monitoring: Opportunities and challenges. *Water Resources Research* 57, no. 12: 1–27. https://doi.org/10.1029/2020wr029500
- Condon, L.E., K.H. Markovich, C.A. Kelleher, J.J. McDonnell, G. Ferguson, and J.C. McIntosh. 2020. Where is the bottom of a watershed? *Water Resources Research* 56, no. 1: 1–9. https://doi.org/10.1029/2019WR026010
- Coon, É.T., and P. Shuai. 2022. Watershed workflow: A toolset for parameterizing data-intensive, integrated hydrologic models. *Environmental Modelling and Software* 157, no. 11: 1-10. https://doi.org/10.1016/j.envsoft.2022.105502
- Dai, Y., W. Shangguan, N. Wei, Q. Xin, H. Yuan, S. Zhang, S. Liu, X. Lu, D. Wang, and F. Yan. 2019. A review of the global soil property maps for earth system models. *The Soil* 5, no. 2: 137–158. https://doi.org/10.5194/soil-5-137-2019

- Dai, Y., N. Wei, H. Yuan, S. Zhang, W. Shangguan, S. Liu, X. Lu, and Y. Xin. 2019. Evaluation of soil thermal conductivity schemes for use in land surface modeling. *Journal of Advances in Modeling Systems* 11: 3454–3473. https://doi.org/10.1139/t04106
- Dai, Y., Q. Xin, N. Wei, Y. Zhang, W. Shangguan, H. Yuan, S. Zhang, S. Liu, and X. Lu. 2019. A global HighResolution data set of soil hydraulic and thermal properties for land surface modeling. *Journal of Advances in Modeling Earth Systems* 11: 2996–3023. https://doi.org/10.1029/2019MS0017842996
- de Graaf, I.E.M., E.H. Sutanudjaja, L.P.H. Van Beek, and M.F.P. Bierkens. 2015. A high-resolution global-scale groundwater model. *Hydrology and Earth System Sciences* 19, no. 2: 823–837. https://doi.org/10.5194/hess-19-823-2015
- de Graaf, I., L. Condon, and R. Maxwell. 2020. Hyper-resolution continental-scale 3-D aquifer parameterization for groundwater modeling. *Water Resources Research* 56, no. 5: 1-14. https://doi.org/10.1029/2019WR026004
- de Pue, J., M. Rezaei, M. van Meirvenne, and W.M. Cornelis. 2019. The relevance of measuring saturated hydraulic conductivity: Sensitivity analysis and functional evaluation. *Journal of Hydrology* 576, no. 9: 628–638. https://doi.org/10.1016/j.jhydrol.2019.06.079
- Enemark, T., L.J.M. Peeters, D. Mallants, and O. Batelaan. 2019. Hydrogeological conceptual model building and testing: A review. *Journal of Hydrology* 569, no. 2: 310–329. https://doi.org/10.1016/j.jhydrol.2018.12.007
- Fan, Y., H. Li, and G. Miguez-Macho. 2013. Global patterns of groundwater table depth. *Science* 339, no. 6122: 940–943. https://doi.org/10.1126/science.1229881
- Fan, Y., G. Miguez-Macho, C.P. Weaver, R. Walko, and A. Robock. 2007. Incorporating water table dynamics in climate modeling: 1. Water table observations and equilibrium water table simulations. *Journal of Geophysical Research Atmospheres* 112, no. 10: 1–17. https://doi.org/ 10.1029/2006JD008111
- Foster, L.M., and R.M. Maxwell. 2019. Sensitivity analysis of hydraulic conductivity and Manning's *n* parameters lead to new method to scale effective hydraulic conductivity across model resolutions. *Hydrological Processes* 33, no. 3: 332–349. https://doi.org/10.1002/hyp.13327
- Gleeson, T., T. Wagener, P. Döll, S. Zipper, C. West, Y. Wada, R. Taylor, B. Scanlon, R. Rosolem, S. Rahman, N. Oshinlaja, R. Maxwell, M.H. Lo, H. Kim, M. Hill, A. Hartmann, G. Fogg, J.S. Famiglietti, A. Ducharne, I.D.G.M. Cuthbert, L. Condon, E. Bresciani, and M.F.P. Bierkens. 2021. GMD perspective: The quest to improve the evaluation of groundwater representation in continental to global scale models. Geoscientific Model Development Discussions 14, no. 4: 1–59. https://doi.org/10.5194/gmd-2021-97
- Gleeson, T., K.M. Befus, S. Jasechko, E. Luijendijk, and M.B. Cardenas. 2016. The global volume and distribution of modern groundwater. *Nature Geoscience* 9, no. 2: 161–164. https://doi.org/10.1038/ngeo2590
- Gleeson, T., N. Moosdorf, J. Hartmann, and L.P.H. Van Beek. 2014. A glimpse beneath earth's surface: GLobal HYdrogeology MaPS (GLHYMPS) of permeability and porosity. *Geophysical Research Letters* 41, no. 11: 3891–3898. https://doi.org/10.1002/2014GL059856
- Gochis, D.J., E.R. Vivoni, and C.J. Watts. 2010. The impact of soil depth on land surface energy and water fluxes in the North American Monsoon region. *Journal of Arid Environments* 74, no. 5: 564–571. https://doi.org/10.1016/j.jaridenv.2009.11.002
- Gratzer, M.C., G.R. Davidson, A.M. O'Reilly, and J.R. Rigby. 2020. Groundwater recharge from an oxbow lake-wetland system in the Mississippi Alluvial Plain. *Hydrological Processes* 34, no. 6: 1359–1370. https://doi.org/10.1002/hyp.13680

- Gupta, S., P. Lehmann, S. Bonetti, A. Papritz, and D. Or. 2021. Global prediction of soil saturated hydraulic conductivity using random forest in a covariate-based GeoTransfer function (CoGTF) framework. *Journal of Advances in Modeling Earth Systems* 13, no. 4: 1-15. https://doi.org/10.1029/2020MS002242
- Hellwig, J., I.E.M. de Graaf, M. Weiler, and K. Stahl. 2020. Large-scale assessment of delayed groundwater responses to drought. *Water Resources Research* 56, no. 2: 1-19. https://doi.org/10.1029/2019WR025441
- Huscroft, J., T. Gleeson, J. Hartmann, and J. Börker. 2018. Compiling and mapping global permeability of the unconsolidated and consolidated earth: GLobal HYdrogeology MaPS 2.0 (GLHYMPS 2.0). *Geophysical Research Letters* 45, no. 4: 1897–1904. https://doi.org/10.1002/2017GL075860
- Jarvis, N., J. Koestel, I. Messing, J. Moeys, and A. Lindahl. 2013. Influence of soil, land use and climatic factors on the hydraulic conductivity of soil. *Hydrology and Earth System Sciences* 17, no. 12: 5185–5195. https://doi.org/10.5194/ hess-17-5185-2013
- Jiang, X.W., L. Wan, X.S. Wang, S. Ge, and J. Liu. 2009. Effect of exponential decay in hydraulic conductivity with depth on regional groundwater flow. *Geophysical Research Letters* 36, no. 24: 1-4. https://doi.org/10.1029/ 2009GL041251
- Jones, J.E., and C.S. Woodward. 2001. Newton-Krylov-multigrid solvers for large-scale, highly heterogeneous, variably saturated flow problems. *Advances in Water Resources* 24, no. 7: 763–774. https://doi.org/10.1016/S0309-1708(00)00075-0
- Kollet, S.J., and R.M. Maxwell. 2008. Capturing the influence of groundwater dynamics on land surface processes using an integrated, distributed watershed model. *Water Resources Research* 44, no. 2: 1–18. https://doi.org/10.1029/2007WR006004
- Kuffour, B., N. Engdahl, C. Woodward, L. Condon, S. Kollet, and R. Maxwell. 2020. Simulating coupled surface-subsurface flows with ParFlow v3.5.0: Capabilities, applications, and ongoing development of an open-source, massively parallel, integrated hydrologic model. Geoscientific Model Development Discussions 13: 1373–1397. https://doi.org/10.5194/gmd-2019-190
- Luo, W., B.P. Grudzinski, and D. Pederson. 2010. Estimating hydraulic conductivity from drainage patterns-a case study in the Oregon Cascades. *Geology* 38, no. 4: 335–338. https://doi.org/10.1130/G30816.1
- Maxwell, R. M., S. J. Kollet, L. E. Condon, S. G. Smith, C. S. Woodward, R. D. Falgout, I. M. Ferguson, et al. 2023. ParFlow Documentation Release 3.12.0. https://parflow.readthedocs.io/en/latest/index.html.
- Maxwell, R.M., and L.E. Condon. 2016. Connections between groundwater flow and transpiration partitioning. *Science* 353, no. 6297: 377–379. https://doi.org/10.1126/science.aaf7891
- Maxwell, R.M., L.E. Condon, and S.J. Kollet. 2015. A high-resolution simulation of groundwater and surface water over most of the continental US with the integrated hydrologic model ParFlow v3. *Geoscientific Model Development* 8: 923–937. https://doi.org/10.5194/gmd-8-923-2015
- Maxwell, R.M. 2013. A terrain-following grid transform and preconditioner for parallel, large-scale, integrated hydrologic modeling. *Advances in Water Resources* 53: 109–117. https://doi.org/10.1016/j.advwatres.2012.10.001
- Maxwell, R.M., and N.L. Miller. 2005. On the development of a coupled land surface and groundwater model. *Developments in Water Science* 55, no. pt 2: 1503–1510. https://doi.org/10.1016/S0167-5648(04)80161-8
- Mcintosh, J.C., M.E. Schlegel, and M. Person. 2012. Glacial impacts on hydrologic processes in sedimentary basins: Evidence from natural tracer studies. *Geofluids* 12: 7–21. https://doi.org/10.1111/j.1468-8123.2011.00344.x

- Mednick, A. C., J. Sullivan, and D. J. Watermolen. 2008. Comparing the Use of STATSGO and SSURGO soils data in water quality modeling: A literature review, http://soildatamart.nrcs.usda.gov/USDGSM.aspx.
- Montzka, C., M. Herbst, L. Weihermüller, A. Verhoef, and H. Vereecken. 2017. A global data set of soil hydraulic properties and sub-grid variability of soil water retention and hydraulic conductivity curves. *Earth System Science Data* 9, no. 2: 529–543. https://doi.org/10.5194/essd-9-529-2017
- O'Neill, M., D. Tijerina, L. Condon, and R. Maxwell. 2021. Assessment of the ParFlow-CLM CONUS 1.0 integrated hydrologic model: Evaluation of hyper-resolution water balance components across the contiguous United States. *Geoscientific Model Development* 14: 7223–7254. https://doi.org/10.5194/gmd-2020-364
- Pan, M. Lettenmaier, D. P., 2023. CW3E WRF-hydro based seasonal water supply forecast system technical notes (Version 20230301). Center for Western Weather and Water Extremes (CW3E), Scripps Institution of Oceanography, University of California San Diego. https://docs.google.com/document/d/17xmIsv9Q9G_ 1BBBPQAMuSdnLNQ90-89t131q5oiKqKQ
- Pelletier, J.D., P.D. Broxton, P. Hazenberg, X. Zeng, P.A. Troch, G.Y. Niu, Z. Williams, M.A. Brunke, and D Gochis. 2016. A gridded global data set of soil, intact regolith, and sedimentary deposit thicknesses for regional and global land surface modeling. *Journal of Advances in Modeling Earth Systems* 8, no. 1: 41–65. https://doi.org/10.1002/2015MS000526
- Peterman, W., D. Bachelet, K. Ferschweiler, and T. Sheehan. 2014. Soil depth affects simulated carbon and water in the MC2 dynamic global vegetation model. *Ecological Modelling* 294, no. 12: 84–93. https://doi.org/10.1016/j.ecolmodel.2014.09.025
- Reinecke, R., A. Wachholz, S. Mehl, L. Foglia, C. Niemann, and P. Döll. 2020. Importance of spatial resolution in global groundwater modeling. *Groundwater* 58, no. 3: 363–376. https://doi.org/10.1111/gwat.12996
- Schaap, M.G., and F.J. Leij. 1998. Database-related accuracy and uncertainty of pedotransfer functions. *Soil Science* 163, no. 10: 765–779.
- Shangguan, W., T. Hengl, J. Mendes de Jesus, H. Yuan, and Y. Dai. 2017. Mapping the global depth to bedrock for land surface modeling. *Journal of Advances in Modeling Earth Systems* 9, no. 1: 65–88. https://doi.org/10.1002/2016MS000686
- Shangguan, W., Y. Dai, Q. Duan, B. Liu, and H. Yuan. 2014. A global soil data set for earth system modeling. *Journal of Advances in Modeling Earth Systems* 6, no. 1: 249–263. https://doi.org/10.1002/2013MS000293
- Soil Survey Staff, Natural Resources Conservation Service (NRCS), United States Department of Agriculture. Soil Survey Geographic (SSURGO) database. https://sdmdataaccess.sc.egov.usda.gov.
- Soil Survey Staff, Natural Resources Conservation Service (NRCS), United States Department of Agriculture. U.S. General Soil Map (STATSGO2). https://sdmdataaccess.sc.egov.usda.gov.

- Srivastava, V., W. Graham, R. Muñoz-Carpena, and R.M. Maxwell. 2014. Insights on geologic and vegetative controls over hydrologic behavior of a large complex basin—Global sensitivity analysis of an integrated parallel hydrologic model. *Journal of Hydrology* 519, no. PB: 2238–2257. https://doi.org/10.1016/j.jhydrol.2014.10.020
- Sutanudjaja, E.H., L.P.H. Van Beek, S.M. De Jong, F.C. Van Geer, and M.F.P. Bierkens. 2014. Calibrating a large-extent high-resolution coupled groundwater-land surface model using soil moisture and discharge data. *Water Resources Research* 50, no. 1: 687–705. https://doi.org/10.1002/2013WR013807
- Tashie, A., T. Pavelsky, L. Band, and S. Topp. 2021. Watershed-scale effective hydraulic properties of the continental United States. *Journal of Advances in Modeling Earth Systems* 13, no. 6: 1-18. https://doi.org/10.1029/2020MS002440
- Tran, H., J. Zhang, J.M. Cohard, L.E. Condon, and R.M. Maxwell. 2020. Simulating groundwater-streamflow connections in the upper Colorado River Basin. *Groundwater* 58, no. 3: 392–405. https://doi.org/10.1111/gwat. 13000
- U.S. Geological Survey. 2003. Principal aquifers of the 48 Conterminous United States, Hawaii, Puerto Rico, and the U.S. Virgin Islands: U.S. Geological Survey National Atlas of the United States. https://water.usgs.gov/ogw/aquifer/map.html.
- Wang, X., and A.M. Melesse. 2006. Effects of STATSGO and SSURGO as inputs on SWAT model's snowmelt simulation. *Journal of the American Water Resources Association* 42, no. 5: 1217–1236. https://doi.org/10.1111/j.1752-1688. 2006.tb05296.x
- van Metre, P.C., S. Qi, J. Deacon, C. Dieter, J.M. Driscoll, M. Fienen, T. Kenney, P. Lambert, D. Lesmes, C.A. Mason, A. Mueller-Solger, M. Musgrove, J. Painter, D. Rosenberry, L. Sprague, A.J. Tesoriero, L. Windham-Myers, and D. Wolock. 2020. Prioritizing river basins for intensive monitoring and assessment by the U.S. Geological Survey. *Environmental Monitoring and Assessment* 192, no. 7: 458. https://doi.org/10.1007/s10661-020-08403-1
- Williamson, T.N., C.J. Taylor, and J.K. Newson. 2013. Significance of exchanging SSURGO and STATSGO data when modeling hydrology in diverse physiographic terranes. *Soil Science Society of America Journal* 77, no. 3: 877–889. https://doi.org/10.2136/sssaj2012.0069
- Xia, Y., M.B. Ek, Y. Wu, T. Ford, and S.M. Quiring. 2015. Comparison of NLDAS-2 simulated and NASMD observed daily soil moisture. Part I: Comparison and analysis. *Journal of Hydrometeorology* 16, no. 5: 1962–1980. https://doi.org/10.1175/JHM-D-14-0096.1
- Xia, Y., M.T. Hobbins, Q. Mu, and M.B. Ek. 2015. Evaluation of NLDAS-2 evapotranspiration against tower flux site observations. *Hydrological Processes* 29, no. 7: 1757–1771. https://doi.org/10.1002/hyp.10299
- Zell, W.O., and W.E. Sanford. 2020. Calibrated simulation of the long-term average surficial groundwater system and derived spatial distributions of its characteristics for the contiguous United States. Water Resources Research 56, no. 8: 1-16. https://doi.org/10.1029/2019WR026724